Neurobiology of Disease

Complete Dissociation of Motor Neuron Death from Motor Dysfunction by Bax Deletion in a Mouse Model of ALS

Thomas W. Gould,[1] Robert R. Buss,[1] Sharon Vinsant,[1] David Prevette,[1] Woong Sun,[2] C. Michael Knudson,[3] Carol E. Milligan,[1] and Ronald W. Oppenheim[1]

[1]Department of Neurobiology and Anatomy and Program in Neuroscience, Wake Forest University, Winston-Salem, North Carolina 27157-1010, [2]Department of Anatomy, College of Medicine, Brain Korea 21, Korea University, Sungbuk-Gu, Seoul 136-705, Korea, and [3]Department of Pathology, The University of Iowa Roy J. and Lucille P. Carver College of Medicine, Iowa City, Iowa 52242

The death of cranial and spinal motoneurons (MNs) is believed to be an essential component of the pathogenesis of amyotrophic lateral sclerosis (ALS). We tested this hypothesis by crossing Bax-deficient mice with mice expressing mutant superoxide dismutase 1 (SOD1), a transgenic model of familial ALS. Although Bax deletion failed to prevent neuromuscular denervation and mitochondrial vacuolization, MNs were completely rescued from mutant SOD1-mediated death. However, Bax deficiency extended lifespan and delayed the onset of motor dysfunction of SOD1 mutants, suggesting that Bax acts via a mechanism distinct from cell death activation. Consistent with this idea, Bax elimination delayed the onset of neuromuscular denervation, which began long before the activation of cell death proteins in SOD1 mutants. Additionally, we show that denervation preceded accumulation of mutant SOD1 within MNs and astrogliosis in the spinal cord, which are also both delayed in Bax-deficient SOD1 mutants. Interestingly, MNs exhibited mitochondrial abnormalities at the innervated neuromuscular junction at the onset of neuromuscular denervation. Additionally, both MN presynaptic terminals and terminal Schwann cells expressed high levels of mutant SOD1 before MNs withdrew their axons. Together, these data support the idea that clinical symptoms in the SOD1 G93A model of ALS result specifically from damage to the distal motor axon and not from activation of the death pathway, and cast doubt on the utility of anti-apoptotic therapies to combat ALS. Furthermore, they suggest a novel, cell death-independent role for Bax in facilitating mutant SOD1-mediated motor denervation.

Key words: **ALS; motoneuron; cell death; denervation; synaptic; axonopathy**

Introduction

Amyotrophic lateral sclerosis (ALS) is an adult-onset motor neuron (MN) disease primarily characterized by degeneration of skeletal muscle-innervating MNs and corticospinal neurons, paralysis, respiratory failure and death (Cleveland and Rothstein, 2001). In contrast to peripheral neuropathies, MN diseases result in the death of affected neurons, presumably through activation of conserved molecular death pathways (Guégan and Przedborski, 2003). Both the morphological and molecular processes through which MN death occurs, as well as whether MN death activation is a required pathogenetic event or merely a consequence of MN dysfunction, remain unresolved. MN death in transgenic models of ALS is heralded by the retraction of presynaptic terminals from muscle, leading to the suggestion that ALS is a "dying-back" axonopathy (Fischer et al., 2004).

Inherited mutations in the superoxide dismutase 1 gene (SOD1) account for 10–20% of familial ALS (FALS), which itself represents 5% of all ALS cases (Rosen et al., 1993). Transgenic animals harboring various mutant SOD1 alleles develop a late-onset MN degenerative disease; the high-expressing SOD1 G93A mutant exhibits behavioral symptom onset at postnatal day 90 (P90)–P100, and death by P120–P140 (Gurney et al., 1994). Mutant but not wild-type SOD1 is found within mitochondria of MNs, and morphologically altered mitochondria are observed early in subtypes of ALS, suggesting that the dysfunction of this organelle may underlie ALS (Wong et al., 1995; Smith et al., 1996; Liu et al., 2004).

Because mitochondrial homeostasis critically regulates neuronal apoptosis (Green and Reed, 1998), the pathological association of mutant SOD1 with mitochondria may result in MN death. Indeed, increases in proapoptotic molecules such as Bax, cytosolic cytochrome C and activated caspases are observed in transgenic models of FALS, and inhibition of caspases or overexpression of Bcl-2 extends survival in these models (Guégan and Przedborski, 2003). The recent report that mutant SOD1 binds the anti-apoptotic factor Bcl-2 provides a direct molecular mechanism by which mutant SOD1 may cause mitochondrial-dependent MN cell death in ALS (Pasinelli et al., 2004).

Although these studies support the existence of both mitochondrial dysfunction and cell death activation in ALS, whether such phenomena are required for MN disease is unclear. Furthermore, the inability of Bcl-2 overexpression to completely rescue

Received April 28, 2006; revised June 30, 2006; accepted July 6, 2006.

This work was supported by National Institutes of Health Grants NS048982 (R.W.O.) and NS368081 (C.E.M.), The Robert Packard Center for Amyotrophic Lateral Sclerosis Research (R.W.O.), and The A. Tab Williams & Family Endowment Fund.

Correspondence should be addressed to Dr. Ronald W. Oppenheim at the above address. E-mail: roppenhm@wfubmc.edu.

DOI:10.1523/JNEUROSCI.2315-06.2006

 0270-6474/06/268774-13$15.00/0

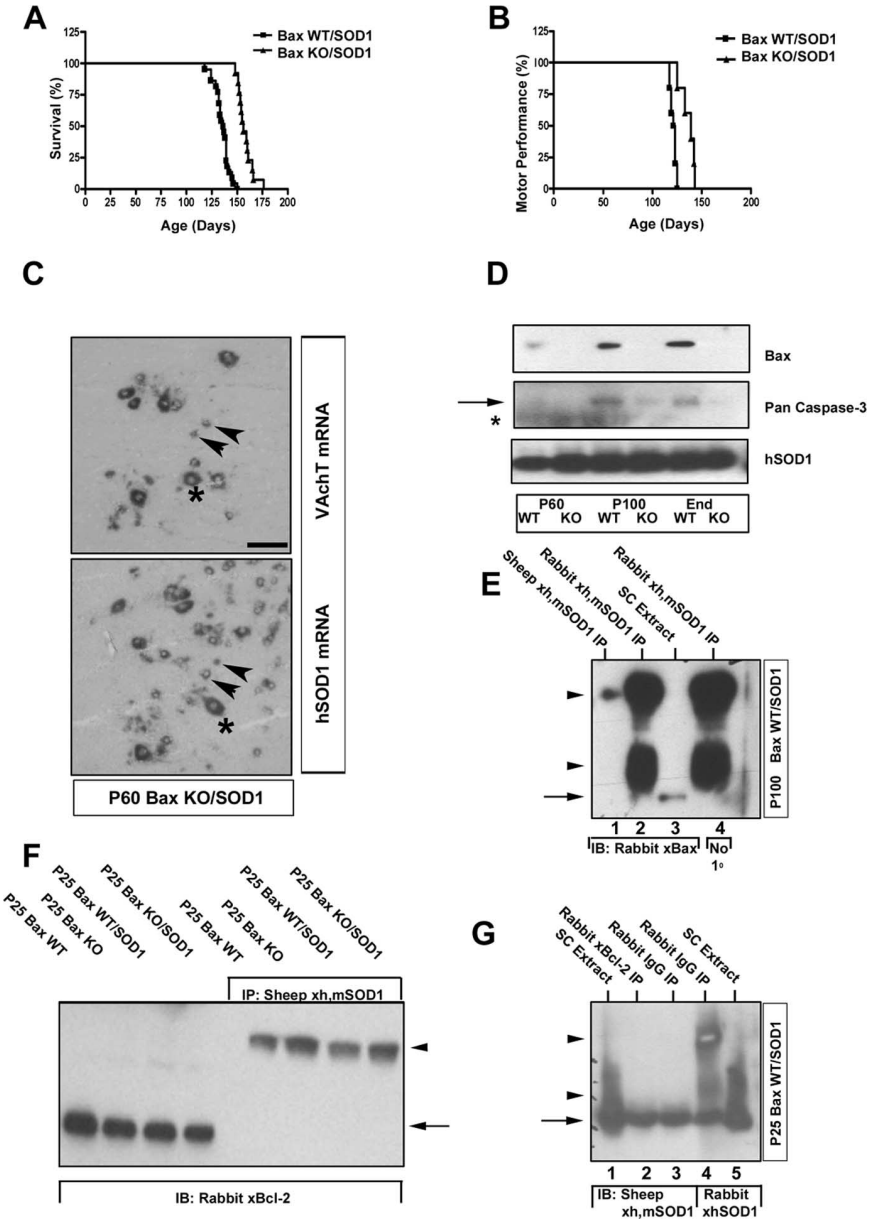

Figure 1. Bax deletion increases lifespan and delays disease onset of SOD1 G93A mutant mice without altering expression of SOD1 or interacting with SOD1. ***A***, Bax KO/SOD1 mutants live longer (higher SOD1 copy number: mean = 137 ± 7 d, $n = 43$ vs 157 ± 9 d, $n = 17$, $p < 0.001$; lower SOD1 copy number: mean = 261 ± 26 d, $n = 73$, vs 283 ± 30 d, $n = 19$, $p < 0.01$) and (***B***) exhibit a decline in motor performance later (119 ± 11 d, $n = 10$ vs 136 ± 13 d, $n = 10$; $p < 0.001$) than Bax WT/SOD1 mutants. ***C***, Mutant SOD1 mRNA is expressed by normal (asterisk) and developmentally rescued, small MNs (arrowheads) that express VAchT mRNA in adjacent sections. Lateral is to the left, medial to the right. Scale bar, 100 μm. ***D***, Expression of Bax, pan-caspase-3 (arrow), and human mutant SOD1 protein in the spinal cord of Bax WT/SOD1 and Bax KO/SOD1 mutants (asterisk denotes a nonspecific band). Immunoblots are representative samples from each genotype (Bax, main effect of genotype: $F_{(1,14)} = 68.5$, $p < 0.0001$; of age: $F_{(2,14)} = 4.05$, $p < 0.05$, $n = 3$; Caspase-3, main effect of genotype: $F_{(1,14)} = 16.0$, $p < 0.005$; of age: $F_{(2,14)} = 50.6$, $p < 0.0001$, $n = 3$; SOD1, no main effects on genotype or age, $n = 3$). ***E***, Antibodies against human/mouse SOD1 (lane 1 or 2, 4) failed to immunoprecipitate Bax protein, which is present in P100 spinal extract (arrow, lane 3). The bottom arrowhead in lane 2 is the IgG light chain, as confirmed by the result in lane 4, after omission of the primary antibody. The top arrowhead is the IgG heavy chain. Image is a representative example from P100 ($n = 4$), although similar results were also obtained at P60 and at end stage. ***F***, Bcl-2 protein is expressed in spinal cord (arrow in first four lanes) but is not observed in P25 spinal cord-derived SOD1 immunoprecipitates (second 4 lanes; arrowhead shows rabbit cross-reactivity to sheep IgG heavy chain, as in ***E***). Image is a representative example from P25 and P45 ($n = 4$). ***G***, SOD1 is present in Bcl-2 and IgG IPs. Both sheep anti-human/mouse SOD1 (arrow, lanes 1–3) and rabbit anti-human SOD1 (arrow, lanes 4–5) are detected in spinal cord-derived Bcl-2 or IgG IPs at every age examined ($n = 3$). Arrowheads denote heavy- and light-chain IgG. IP, Immunoprecipitate.

MNs in FALS mutant mice suggests two opposing yet plausible interpretations: cell death activation causes MN dysfunction, and excess Bcl-2 extends lifespan by attenuating cell death; cell death reflects MN dysfunction and Bcl-2 extends lifespan by alternative mechanisms (Chen et al., 1997). Dissociating cell death from mitochondrial dysfunction and/or from disease would thus be instrumental in testing whether either phenomenon is required or dispensable for ALS pathogenesis.

To begin to address this question, we took advantage of mice deficient in the proapoptotic protein, Bax (Knudson et al., 1995). Bax-null mutant mice are viable and exhibit grossly normal locomotor activity, yet contain twice the number of MNs because of complete inhibition of developmental cell death (Sun et al., 2003). All original and most rescued MNs project axons through the ventral root into muscle-specific peripheral nerves and into muscle (R. R. Buss and R. W. Oppenheim, unpublished observation).

Materials and Methods

Animals and histology. All animal experiments conformed to National Institutes of Health guidelines and were approved by the Wake Forest University Animal Care and Use Committee; protocol #A02-176. To minimize differences caused by strain background, we crossed female Bax heterozygotes (maintained on a C57BL/6 background) with male SOD1+ mice [B6SJL-TgN(SOD1-G93A)1Gur; The Jackson Laboratory, Bar Harbor, ME] to generate F1 Male SOD1+, Bax heterozygotes. These mice were backcrossed to female Bax heterozygotes to generate 10 F2 Male SOD1+, Bax heterozygote males, which were backcrossed again to father the litters used for analysis. Genotyping was performed with standard primers against mutant SOD1 and Bax (Gurney et al., 1994; Knudson et al., 1995). End stage was determined as the time at which an animal could no longer right itself within 30 s after being placed on its back. A decline in motor function was measured as the time at which animals could no longer maintain 11 rpm on a rotarod. Analysis of the morphology of dying cells and measurement of the area of MN cell bodies was performed on spinal-cord sections cut at 10 μm and stained with thionin (Sigma, St. Louis, MO) after perfusion with Bouin's fixative. Somata were traced and analyzed with Scion (Frederick, MD) Image software. For studies with yellow fluorescent protein (YFP)-expressing mice, Bax WT/SOD1 animals were crossed with the B6.Cg-Tg(Thy1-YFPH)2Jrs/J line (The Jackson Laboratory).

Immunohistochemistry. For counting innervated synapses, consecutive 40-μm-thick cross sections of paraformaldehyde-fixed, sucrose-embedded medial gastrocnemii (MGs) were cut and stained with antibodies against synaptophysin (Dako, High Wycombe, UK) and α-bungarotoxin (Sigma). Every third section was analyzed and at least 600 nicotinic acetylcholine receptor (nAchR) clusters were examined per animal. In some cases, antibodies to neurofilament light chain (NF-L) (Chemicon, Temecula, CA) were also used. For counting SOD1-positive aggregates, 10-μm-thick sections of lumbar spinal cord were labeled with a sheep

polyclonal antibody against human/mouse SOD1 (Calbiochem, La Jolla, CA). Glia were identified with anti-glial fibrillary acidic protein (GFAP) antibodies (Chemicon) and anti-S100 antibodies (Dako). Presynaptic mutant SOD1 immunostaining was analyzed confocally [Carl Zeiss (Oberkochen, Germany) Laser Scanning System 510].

In situ *hybridization*. Digoxygenin-labeled riboprobes were made with primers against GFAP (131–1040, GenBank accession number NM010277), vesicular acetylcholine transporter (VAchT; 794–1598, GenBank accession number AF019045), and human SOD1 (CATCAGCCCTAATCCATCTGA, CGCGACTAACAATCAAAGTGA) and hybridized to fresh-frozen tissue sections as described previously (Gould and Oppenheim, 2004). The number of VAchT-positive MNs was quantified by counting the total number of mRNA-positive, Hoechst 33342-stained nuclei in the lumbar spinal cord, the rostral-caudal limits of which were determined by hindlimb retrograde labeling (Sun et al., 2003) (Gould and Oppenheim, unpublished observations). GFAP-positive astrocytes were quantified by counting the number of mRNA-positive, Hoechst-stained nuclei in the ventral horn per section (five sections per animal examined).

Immunoblotting. The ventral half of the lumbar spinal cord and the sciatic nerve were dissected and proteins extracted by sonication for 45 s in 25 mM Tris, pH 7.6, 150 mM NaCl, 20 mM EDTA, and 1% NP-40, supplemented with 1× protease inhibitors (Sigma). Thirty to 100 μg of protein (1 μg protein for SOD1 probing) were loaded onto 10–12% SDS-containing gels and membranes were probed with antibodies against Bax (rabbit; Cell Signaling, Beverly, MA), caspase-3 (mouse-anti-CPP32; Biomeda, Foster City, CA), human- or mouse-specific SOD1 (kindly provided by Ian Hendry, John Curtin School of Medical Research, Canberra, Australia), human/mouse SOD1 (sheep; Calbiochem), Bcl-2 (rabbit; Fitzgerald Industries, Concord, MA) synaptophysin (rabbit; Dako), growth-associated protein-43 (GAP-43; rabbit; kindly provided by P. Caroni, Friedrich Miescher Institut, Basel, Switzerland) and activated caspase-3 (CM1; BD Biosciences, San Jose, CA). Mouse SOD1 is not detected by the sheep antibody on immunoblots of protein extract prepared from mice overexpressing mutant SOD1, on account of its significantly greater affinity to human versus mouse SOD1 (supplemental Fig. 1, available at www.jneurosci.org as supplemental material). Western blot data were repeated on three different groups of animals and quantified by densitometry on a Bio-Rad (Hercules, CA) gel documentation system (Gel Doc 2000) and subjected to two-way ANOVA (genotype and age).

Immunoprecipitation. Five-hundred micrograms of ventral lumbar spinal cord-derived protein extract was precleared twice for 45 min with 40 μl of protein A-conjugated agarose beads (Sigma), rotated at 4°C for 4–16 h with antibodies against Bcl-2 (5 μl, rabbit; Fitzgerald Industries), SOD1 [5 μl, sheep-anti human/mouse (Calbiochem); 5 μl, rabbit anti-human (from Ian Hendry); 4.5 μg, rabbit anti-human/mouse (Stressgen Biotechnology, Victoria, British Columbia, Canada)], Bax (5 μl, rabbit; Cell Signaling), synaptophysin (50 μl, rabbit; Dako), or IgG (5 μg, rabbit; Jackson ImmunoResearch, West Grove, PA). Eighty microliters of beads were added and samples were rotated at 4°C for 8 h, rinsed, and boiled for 5 min in 2× Laemmli buffer before being loaded onto 10–12% SDS gels.

Subcellular fractionation. Ventral spinal cord or sciatic, peroneal, and tibial nerve derived from P30 Bax WT/SOD1 or Bax KO/SOD1 mutants was minced (containing ventral roots) in homogenization buffer containing 255 mM sucrose, 1 mM EDTA, protease inhibitors, and 20 mM HEPES, pH 7.4, and then disrupted with a hand-held homogenizer at 15,000 rpm for 1 min. Homogenates were initially spun at 1000 × *g* for 5 min, and the resulting supernatant was then centrifuged at 17,000 × *g* for 20 min to obtain a crude mitochondrial pellet. The second supernatant was centrifuged at 100,000 × *g* for 1 h in an Optima TLX ultracentrifuge, yielding the cytosolic fraction (Beckman Coulter, Fullerton, CA).

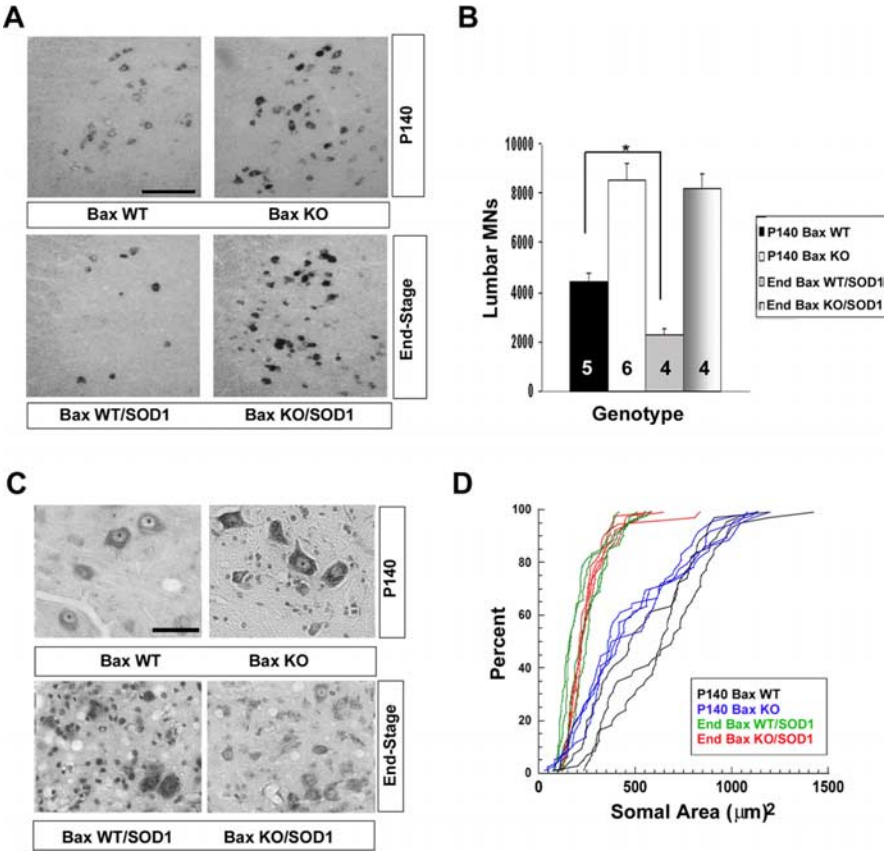

Figure 2. Bax deletion completely rescues the number but not the size of MNs from mutant SOD1-mediated toxicity. ***A***, Lumbar spinal-cord cross sections show that in contrast to end-stage Bax WT/SOD1 mutants (left), the number of VAChT mRNA-expressing MNs is not reduced in end-stage Bax KO/SOD1 mutants, compared with age-matched Bax KO controls. ***B***, Quantitative representation of this data in the entire lumbar spinal cord; $*p < 0.01$, one-way ANOVA. Error bars indicate SDs. ***C***, Images and (***D***) cumulative size distribution of the cross-sectional area of lumbar MN cell bodies in end-stage Bax WT/SOD1 and Bax KO/SOD1 mutants, compared with age-matched controls, reveal atrophy of remaining MNs in both mutants. Means in ***D*** are as follows: Bax WT, 591 ± 264 μm^2; Bax KO, 476 ± 286 μm^2; Bax WT/SOD1, 229 ± 108 μm^2; Bax KO/SOD1, 246 ± 108 μm^2; $p < 0.01$; Bax WT versus Bax WT/SOD1, Bax KO versus Bax KO/SOD1, 100 MNs per animal, $n = 4$ in each group. Each line in (***D***) represents an individual animal. Scale bars: ***A***, 250 μm; ***C***, 100 μm.

Axon counts and ultrastructural analysis. Animals were perfused transcardially with 2% paraformaldehyde and 2% glutaraldehyde in sodium cacodylate buffer, and ventral spinal cord, nerve, and muscles were postfixed in 2% osmium tetroxide, dehydrated, and embedded in Araldite 502. The total number of myelinated axons in fourth lumbar ventral root (L4 VR) and MG nerves was counted in 1-μm-thick sections stained with toluidine blue. The axonal diameter was measured in Scion Image. Vacuolization was analyzed in 1-μm-thick sections of the ventral spinal cord. Unmyelinated axons were examined in ultrathin sections of the L4 ventral root. Mitochondrial area and morphology in ultrathin sections of the MG containing neuromuscular junctions were analyzed in Scion Image.

Data analysis. Statistical significance of survival data was determined with a logrank test. Student's *t* test was used to determine differences in the total number of nAChRs, the percentage of mutant SOD1, YFP double-labeled MNs, and the area and percent vacuolization of presyn-

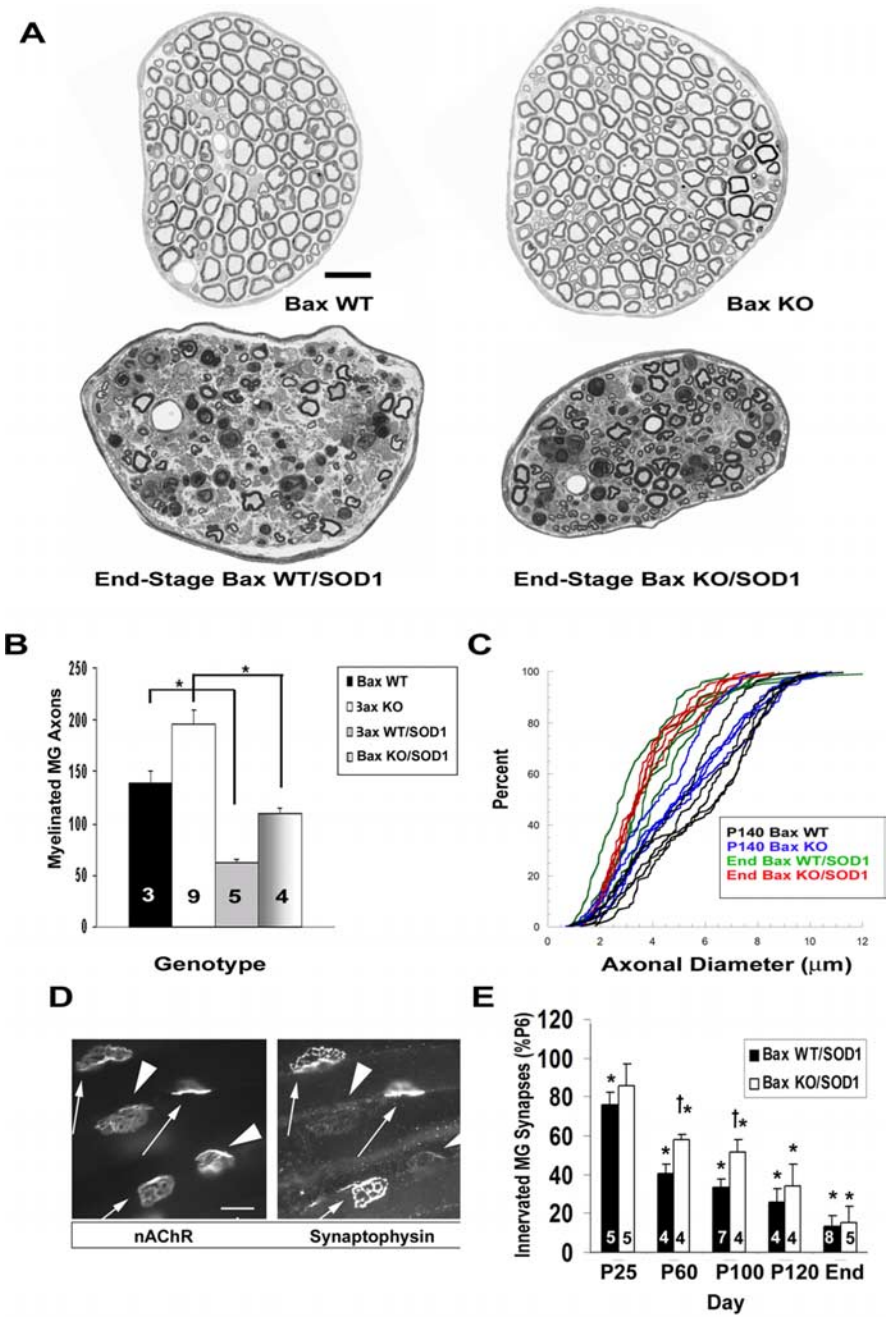

Figure 3. Bax deletion delays but fails to stop distal denervation in SOD1 mutants. ***A***, Representative 1-μm-thick sections of the MG nerve of end-stage Bax WT/SOD1 and Bax KO/SOD1 mutants and age-matched controls. ***B***, Both mutants exhibit a significant reduction of myelinated axons in end-stage MG nerve, relative to control, $^*p < 0.01$. ***C***, Cumulative size distribution of the diameter of remaining myelinated axons in the MG of end-stage Bax WT/SOD1 and Bax KO/SOD1 mutants, relative to age-matched control, reveals atrophy of remaining axons in both mutants. Means are as follows: Bax WT, 5.6 $\pm$ 0.5 μm; Bax KO 5.0 $\pm$ 0.4 μm; Bax WT/SOD1, 3.8 $\pm$ 0.5 μm; Bax KO/SOD1, 3.7 $\pm$ 0.1 μm; Bax WT versus Bax WT/SOD1, $p < 0.001$; Bax KO versus Bax KO/SOD1, $p < 0.01$; $n = 3$ in each group. Each line represents an individual animal. ***D***, Images and (***E***) counts of innervated NMJs in the MG in Bax WT/SOD1 and Bax KO/SOD1 at various ages. Fully and partially innervated nAchR clusters denoted by arrows and arrowheads, respectively, in ***D***. Scale bars: ***A***, 20 μm; ***D***, 10 μm. $^*p < 0.05$ (***E***), respective SOD1 versus P6 SOD1 mutants; $^\dagger p < 0.01$ (***E***), Bax KO/SOD1 versus age-matched Bax WT/SOD1 mutants. Error bars indicate SDs.

aptic mitochondria. One-way ANOVA was used to test differences, between genotypes, in the total number of lumbar VAChT mRNA-positive MNs, the somal area of MNs and the diameter of L4 VR and MG axons. Two-way ANOVA determined significant differences, between age and genotype, in mean optical density (immunoblots), total mRNA-positive cells per section (astrocyte numbers), and total aggresomes per section (mutant SOD1-immunoreactive MNs). *Post hoc* comparisons between groups used the Tukey–Kramer test for multiple comparisons. In all tests, $p < 0.05$ was considered significant. We used Statistica 6.0 for analysis (StatSoft, Tulsa, OK).

Results

Bax deletion prolongs survival and completely blocks cell death in SOD1 mutants

To examine the effect of the proapoptotic gene Bax on MN survival in a transgenic model of ALS, we crossed high-expressing and low-expressing SOD1 G93A mutant mice with Bax knock-out (KO) mice (Knudson et al., 1995). Compared with Bax +/−SOD1 mutants and Bax +/+SOD1 mutants, Bax KO/SOD1 mutants lived 14.6% longer (Fig. 1*A*). Because Bax heterozygosity failed to influence lifespan differences, we pooled Bax +/−SOD1 mutants together with Bax +/+SOD1 mutants [referred to as Bax wild-type (WT)/SOD1 mutants]. In addition to living longer, Bax KO/SOD1 mutants maintained 11 rpm on the rotarod for a significantly longer period of their lifespan than Bax WT/SOD1 mutants (14.3% increase) (Fig. 1*B*). These results show that Bax deletion, similar to Bcl-2 overexpression (14.6% increase in survival, 19.3% increase in disease onset) (Kostic et al., 1997), increases longevity of SOD1 mutant mice by delaying the onset of motor decline, rather than by increasing survival after disease onset.

Bax deletion does not promote survival of SOD1 mutants by reducing the level of human mutant SOD1 expression in lumbar ventral spinal cord extracts (Fig. 1*D*). Although overall levels of mutant SOD1 protein are unchanged, we wanted to verify that developmentally rescued MNs, which overlap in size with small MNs in the spinal cord and hence are referred to as "atrophic," also expressed mutant SOD1 (Sun et al., 2003). Many small cells in the lumbar ventral horn expressed human SOD1 mRNA in Bax KO/SOD1 mutants, and adjacent sections hybridized with a riboprobe against the VAchT, a cholinergic marker, suggest that these small mutant SOD1 mRNA-positive cells are MNs (Fig. 1*C*).

To examine whether Bax deletion increased lifespan of SOD1 mutants by perturbation of a direct physical interaction between Bax and SOD1, we performed immunoprecipitation experiments with Bax and SOD1 antisera. Precipitation of lumbar ventral spinal cord, sciatic nerve, or hindlimb muscle extracts with several different antibodies recognizing only human mutant SOD1 or both human mutant and mouse WT SOD1 failed to provide evidence for direct physical interaction (Fig. 1*E*). Because a recent report demonstrated that both WT and mutant SOD1 bind Bcl-2

Table 1. Number and percentage of myelinated axons in end-stage SOD1 mutants

Nerve	Bax WT/SOD1	Bax KO/SOD1
Femoral	264 ± 81 (49%) ($n = 4$)	472 ± 14 (61%) ($n = 4$)
MG	62 ± 5 (50%) ($n = 5$)	109 ± 11 (58%) ($n = 5$)
Phrenic	142 ± 102 (55%) ($n = 5$)	127 ± 30 (40%) ($n = 5$)
L4 VR	614 ± 135 (57%) ($n = 4$)	1053 ± 181 (58%) ($n = 4$)
Saphenous	783 ± 73 (98%) ($n = 5$)	951 ± 55 (104%) ($n = 4$)

%, Percentage of age-matched controls.

Table 2. Number and percentage of myelinated axons in P100 and end-stage SOD1 mutants

Nerve	Bax WT/SOD1	Bax KO/SOD1
P100 L4 VR	706 ± 99 (66%) ($n = 7$)	1536 ± 169 (84%) ($n = 3$)
End-stage L4 VR	614 ± 135 (57%) ($n = 4$)	1053 ± 181 (58%) ($n = 4$)
P100 L4 MG	76 ± 16 (61%) ($n = 7$)	140 ± 2 (75%) ($n = 3$)
End-stage L4 MG	62 ± 5 (50%) ($n = 5$)	109 ± 11 (58%) ($n = 5$)

%, Percentage of age-matched controls.

(Pasinelli et al., 2004), and because Bax and Bcl-2 interaction is observed in Bax WT/SOD1 mutant spinal cord extracts (Vukosavic et al., 1999), we found it surprising that Bax and SOD1 failed to coprecipitate at any age. Therefore, we looked for an interaction between Bcl-2 and SOD1. Using a sheep antibody that recognizes both human mutant and mouse WT SOD1 and that exhibits minor cross-reactivity to the heavy chain of rabbit IgG, and using the same rabbit antibody against mouse Bcl-2 as reported by Pasinelli et al. (2004), we were unable to detect Bcl-2 immunoreactivity in SOD1 immunoprecipitates of spinal cord extract at any age (Fig. 1*F*). Similar experiments using rabbit antibodies against specifically either human SOD1 or mouse SOD1 for immunoprecipitation were difficult to interpret because of the similarity in size between the IgG light chain (25 kDa) and Bcl-2 (26 kDa; data not shown). We detected synaptophysin in sheep anti-SOD1 precipitates, suggesting that the failure to observe Bcl-2 is not because of poor immunoprecipitation by this antibody (see Fig. 9). Interestingly, although we failed to detect Bcl-2 in SOD1 precipitates, we found mutant SOD1 in spinal cord-derived Bcl-2 immunoprecipitates, similar to Pasinelli et al. (2004) (Fig. 1*G*). However, we also detected SOD1 bands after immunoprecipitation with rabbit IgG, even after extensive preclearing (Fig. 1*G*); similar false-positive data with preimmune serum was reported by Kirkinezos et al. (2005). Together, these data suggest that the extension in lifespan of SOD1 mutants conferred by Bax deletion is not caused by differences in expression of mutant SOD1 or by manipulations of interactions between Bax or Bcl-2 and SOD1.

To examine the effects of Bax deletion on cell death in FALS mutant mice, we compared levels of cell death proteins in lumbar ventral spinal cord extract and examined the number and size of MNs in Bax WT/SOD1 and Bax KO/SOD1 mutants. We measured levels of proapoptotic factors at P60, before death activation, at P100, the peak of death activation, and at the end stage of disease (Chiu et al., 1995). In contrast to extracts prepared from Bax KO/SOD1 mutants that failed to exhibit Bax immunoreactivity, samples from Bax WT/SOD1 mutants contained increasing amounts of Bax protein during the period of MN death (Fig. 1*D*). The expression of a cell death executor, caspase-3, peaked at P100 in Bax WT/SOD1 and to a lesser extent in Bax KO/SOD1 mutants (Fig. 1*D*). However, we were unable to detect increases of activated caspase-3 in either genotype by immunoblotting (data not shown) (Migheli et al., 1999) (but see Pasinelli et al., 2000; Kang et al., 2003).

To determine whether MNs undergo apoptosis as a result of mutant SOD1-mediated toxicity, we systematically examined Nissl-stained sections of both P120 and end-stage lumbar spinal cord of both genotypes. We observed many cells that contained large perinuclear vacuoles in the ventral horn at P120 (data not shown), but never cells with pyknotic nuclei, a hallmark of apoptosis, in either genotype at P120 or at end stage (supplemental Fig. 1, available at www.jneurosci.org as supplemental material) (but see Guégan and Przedborski, 2003). Therefore, we quantified overall numbers of lumbar MNs at end stage in both genotypes by counting the number of VAchT mRNA-positive, Hoechst-stained nuclei in the ventral horn (Fig. 2*A*). This counting technique reliably quantifies lumbar MNs in both WT and transgenic animals with altered numbers of MNs, based on comparisons to the total number of axons in lumbar ventral roots (Sun et al., 2003) (Gould and Oppenheim, unpublished observations). In contrast to Bax WT/SOD1 mutants, which exhibited a ~50% reduction in MN numbers at end stage, Bax KO/SOD1 mutants retained all MNs at end stage (Fig. 2*B*). We also observed a complete rescue of cervical MNs in end-stage Bax KO/SOD1 mutants (data not shown). However, we found a marked decrease in the somal area of remaining MNs in end-stage mutants of both genotypes, compared with age-matched Bax WT and Bax KO controls, consistent with the idea that these cells have withdrawn from their target and atrophied (Fig. 2*C*,*D*) (supplemental Fig. 1, available at www.jneurosci.org as supplemental material).

Bax deletion fails to inhibit but delays neuromuscular denervation

To confirm the possibility that MN axons withdraw from their target in both genotypes, we counted the number of myelinated axons and innervated synapses in the MG nerve and muscle, respectively. Although Bax KO animals contained an initially higher number of myelinated MG axons than Bax WT, the number at end stage in Bax WT/SOD1 and Bax KO/SOD1 mutants is reduced by a similar percentage (Fig. 3*A*,*B*; Table 1). Similar to the atrophy of remaining cell bodies, the distal axonal diameter of myelinated MG axons is diminished in end-stage Bax WT/SOD1 and Bax KO/SOD1 mutants, relative to Bax WT or Bax KO (Fig. 3*C*). We also examined the phrenic and femoral nerves and found a similar percent reduction in the number of myelinated axons in both genotypes at end stage; counts of the saphenous nerve, which contains only sensory afferent axons, however, remained unaffected (Table 1).

Because the MG nerve consists of both motor and proprioceptive sensory axons, and Bax KO animals contain additional sensory axons rescued earlier from developmental cell death, we wanted to rule out the possibility that distal MG nerve counts were not biased by changes in the number of proprioceptive axons, which are the subtype of sensory axon most likely affected in ALS (Heads et al., 1991). Therefore, we counted the number of innervated postsynaptic nAChR clusters in the MG and found that neither the total number (Bax WT, 4931 ± 342; Bax KO, 5134 ± 449; $p > 0.5$; $n = 3$), nor the percentage of innervated nAChR clusters (100% in both genotypes) was significantly different. We also observed that all innervated neuromuscular junctions (NMJs) are innervated in P6 Bax WT/SOD1 and Bax KO/SOD1 mutants, suggesting that innervation during development proceeds normally. In contrast, end-stage Bax WT/SOD1 and Bax KO/SOD1 mutants exhibited a marked loss of fully innervated NMJs in the MG, between 10–20% of P6 values (Fig. 3*D*,*E*). These numbers confirm that Bax KO/SOD1 mice, in which MNs fail to die, nevertheless display a reduction of neuromuscular innervation similar to Bax WT/SOD1 mutants, and

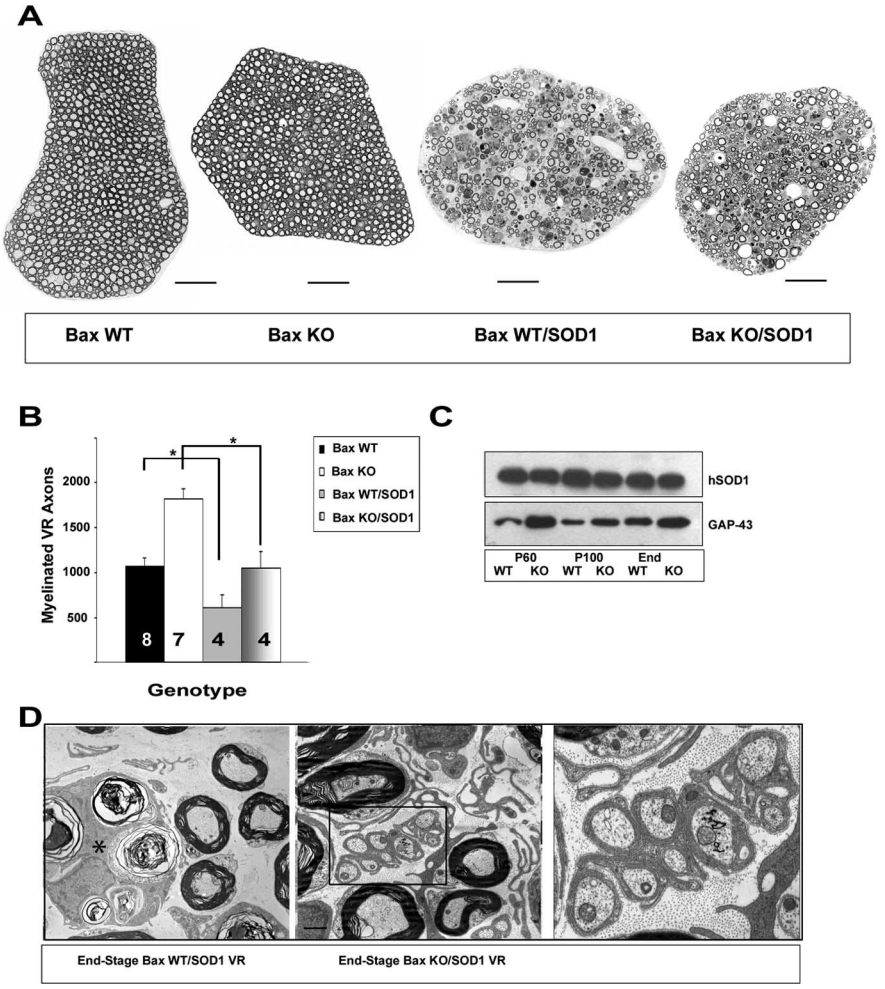

Figure 4. Reduction in the number of fully myelinated axons in the ventral root of Bax KO/SOD1 mutants. ***A***, Representative 1-μm-thick sections of the L4 VR of end-stage Bax WT/SOD1 and Bax KO/SOD1 mutants and age-matched controls. Scale bars: Bax WT, Bax KO, 67 μm; Bax WT/SOD1, Bax KO/SOD1 mutants, 50 μm . ***B***, Both mutants exhibit a significant reduction of myelinated axons in end-stage L4 VR, relative to control; $^*p < 0.01$, one-way ANOVA. Error bars indicate SDs. ***C***, Increased GAP-43 but not mutant SOD1 expression in sciatic nerve protein extracts of Bax KO/SOD1 mutant [mean: 1.58 $\pm$ 0.45 optical density units (ODU), Bax WT/SOD1 versus 2.81 $\pm$ 0.88 ODU, Bax KO/SOD1 mutant; main effect of genotype: $F_{(1,14)} = 17.4$; $p < 0.001$; $n = 3$]. ***D***, Electron micrographs of end-stage Bax WT/SOD1 (left) or Bax KO/SOD1 (middle and right) L4 VR. The asterisk in the left image shows degenerating axons engulfed by a phagocytic cell. The box in the middle image contains a representative image of a group of eight unmyelinated axons wrapped by a glial cell process and is enlarged in right image. Scale bar, 1 μm.

suggest that this final level of innervation itself is a marker of disease.

If Bax KO/SOD1 mice display the same overall extent of distal denervation as Bax WT/SOD1 mutants, why does Bax deletion increase lifespan? Indeed, in a transgenic model of prion disease, Bax deletion failed to block the loss of target innervation of cerebellar granule neurons or to increase lifespan, despite reducing granule cell death (Chiesa et al., 2005). The finding that initial and final numbers of innervated synapses in the MG are similar in both genotypes, together with the finding that Bax KO/SOD1 mutants live 15% longer than Bax WT/SOD1 mutants, suggests that the rate of neuromuscular denervation is decreased over time in Bax KO/SOD1 mutants. Consistent with this interpretation, we found that P100 Bax KO/SOD1 mutants exhibited significantly more MG axons and innervated NMJs than P100 Bax WT/SOD1 mutants (Table 2; Fig. 3*E*). We also failed to observe a difference in the percentage of innervated NMJs at timepoints normalized to lifespan (80% lifespan: P100 Bax WT/SOD1, 34 $\pm$ 7%; P120 Bax KO/SOD1, 35 $\pm$ 4%; $p > 0.8$; $n = 4$) (Fig. 3*E*).

We next determined whether Bax deficiency delayed the reduction of distal axons and innervated synapses by delaying the onset and/or the rate of denervation. To distinguish these possibilities, we first counted innervated NMJs in the MG at various ages after P6. Whereas previous studies noted a ~40% loss of innervation at P45 in Bax WT/SOD1 mutants (Kennel et al., 1996; Frey et al., 2000; Fischer et al., 2004; Ligon et al., 2005), we detected a significant decrease as early as P25 in Bax WT/SOD1, but not Bax KO/SOD1 mutants (Fig. 3*E*), suggesting that Bax deletion delays the onset of denervation. Bax KO/SOD1 mutants begin to exhibit a loss of innervation at P45 and continue to contain more fully innervated NMJs at subsequent ages than Bax WT/SOD1 mutants, until P120 (Fig. 3*E*) (data not shown). Additionally, we failed to observe differences between genotypes in the rate of loss of innervated NMJs between intermediate timepoints (data not shown). These data support the interpretation that Bax deletion reduces the loss of neuromuscular innervation in SOD1 mutants by delaying the onset rather than the rate of this loss.

Bax deletion delays but fails to prevent demyelination of ventral root motor axons

We next examined whether the reduction of myelinated axons in Bax KO/SOD1 mutants was restricted to distal segments by counting the number of axons in the L4 ventral root, which is composed exclusively of motor axons. Similar to results obtained from other distal nerves, the percentage of remaining L4 ventral root axons at end stage is equivalent in both genotypes (Fig. 4*A*,*B*; Table 2). Axonal diameter is also similarly reduced in both mutants, relative to control (data not shown). Analysis of P100 versus end-stage L4 ventral root axon numbers revealed that Bax deletion delays the loss of both distal and proximal myelinated axons (Table 2). Because Bax KO L4 ventral roots contain significant increases in the number of both myelinated and unmyelinated axons versus Bax WT (~1.3-fold of the latter; Buss and Oppenheim, unpublished observations), we examined whether myelinated axon counts of end-stage Bax KO/SOD1 mutants might have included some of these originally unmyelinated axons attempting to myelinate, or whether changes in the numbers of collateral (nodal) axon sprouts could be observed, as they have been in sporadic ALS (Hanyu et al., 1982). To investigate these issues, we examined electron photomicrographs of end-stage L4 ventral roots from Bax WT/SOD1 and Bax KO/SOD1 mutants as well as of age-matched Bax KO and Bax WT controls. We noticed many small groups of axons multiply wrapped in glial cell processes in Bax KO/SOD1 mutants, but only single axons of this type in Bax KO controls and neither type in Bax WT or Bax WT/SOD1 mutants (Fig. 4*D*). These unmyelinated axons could be either axonal sprouts from denervated MNs

or axons of developmentally rescued MNs. Because unmyelinated axons in Bax KO ventral roots seldom appear in groups, and are far fewer in overall number than in Bax KO/SOD1 ventral roots (Bax KO/SOD1, 43 ± 24; Bax KO, 10 ± 4; $n = 2$; eight fields at 3150×), we favor the idea that they are sprouts derived from denervated MNs. We observed significant increases in GAP-43 protein expression in Bax KO/SOD1 versus Bax WT/SOD1 mutants, supporting this interpretation (Fig. 4*C*).

In addition to containing completely denervated synapses, both genotypes exhibited partially innervated synapses, including endplates with intense but partial innervation as well as those with very light but complete innervation (Fig. 3*D*). Interestingly, end-stage Bax KO/SOD1 mutants contained markedly higher levels of partially innervated synapses in the MG than Bax WT/SOD1 mutants (59 vs 24%; $p > 0.01$; $n = 4$). This finding supports the idea that unmyelinated axons in end-stage Bax KO/SOD1 are sprouts from denervated axons, because partial denervation has been shown to stimulate collateral sprouting (Lubischer and Thompson, 1999). Alternatively, increases in partially innervated synapses in Bax KO/SOD1 mutants may reflect enhanced terminal sprouting. Because we find very limited evidence of sprouts extending past partially innervated AChR clusters, we favor the hypothesis that Bax deletion attenuates denervation, which results in increased collateral sprouting from partially denervated axons.

Bax deletion delays the accumulation of mutant SOD1 in MNs that occurs after denervation

Because SOD1-mediated toxicity to MNs may result from a propensity to form altered multimeric conformations, including detergent-resistant high-molecular-weight complexes (Bruijn et al., 1998; Johnston et al., 2000), we tested whether Bax deletion prolonged survival by affecting this process. We observed mutant SOD1 immunoreactivity in the ventral horn of both Bax WT/SOD1 and Bax KO/SOD1 mutants, which peaked at P60 and colocalized with the MN marker ChAT (Fig. 5*A–C*) (data not shown). The cytoplasmic localization of SOD1 immunostaining suggests that it represents mutant SOD1 aggregates that escape proteosome-mediated degradation because of their size and are tracked to the microtubule organizing center (Johnston et al., 1998). We first detected mutant SOD1-positive inclusions at P30 in Bax WT/SOD1 mutants and at P40 in Bax KO/SOD1 mutants, similar to an earlier report, which detected high-molecular-weight immunoreactive species of mutant SOD1 at P30 by immunoblotting (Johnston et al., 2000). Interestingly, the number of MNs with aggregates decreased dramatically in Bax WT/SOD1 but not Bax KO/SOD1 mutants over time, consistent with the inhibition of MN death in Bax KO/SOD1 mutants (Fig. 5*A*, *C*). By P100 in Bax WT/SOD1 mutants, the preponderance of mutant SOD1 immunoreactivity was restricted to the rims of clear, vacuolated profiles (data not shown).

Because a recent study reported that MNs secrete mutant SOD1 (Urushitani et al., 2006), denervated MNs might accumulate SOD1 because of a reduced ability to export this toxic pro-

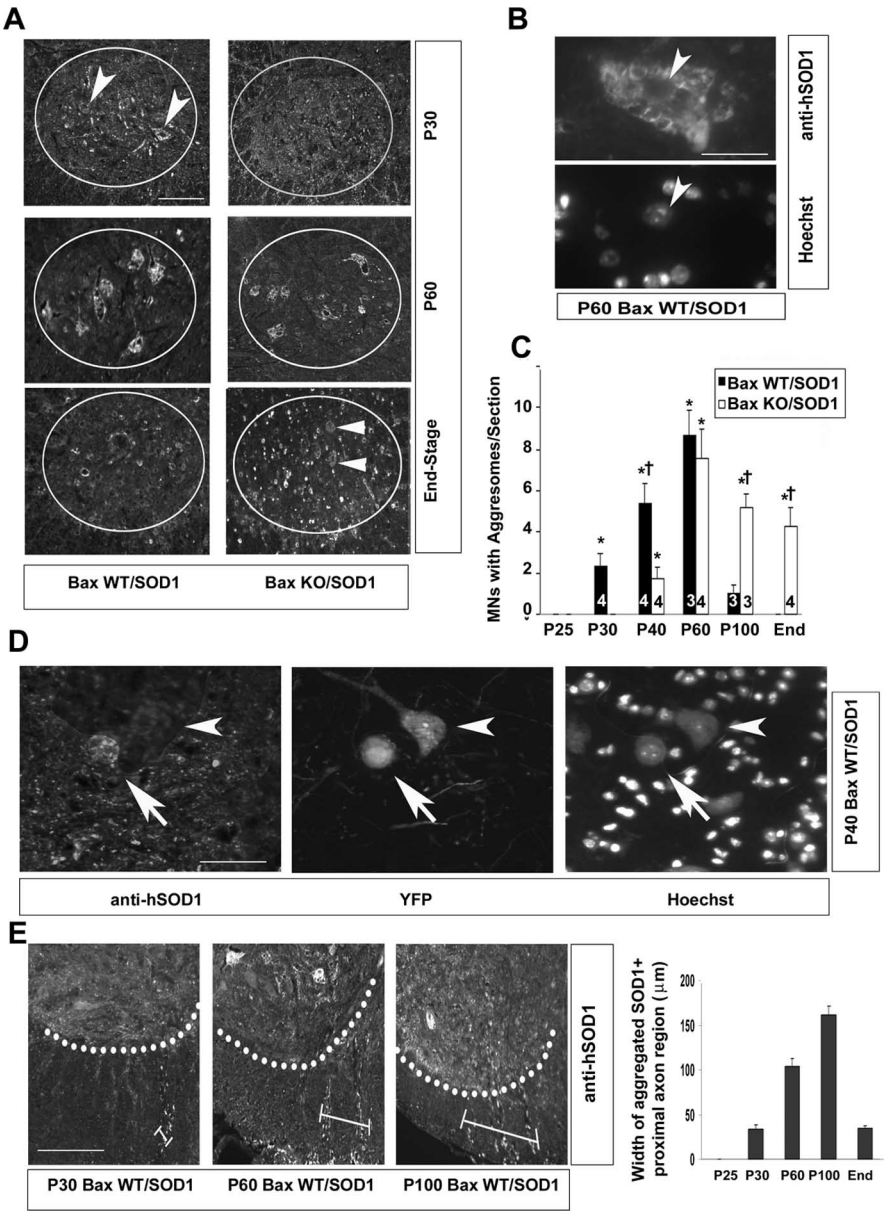

Figure 5. Bax deletion delays the formation of mutant SOD1-positive aggregates in MNs, which occurs after the onset of neuromuscular denervation. ***A***, ***C***, Mutant SOD1 is expressed at P30 in lumbar MNs in Bax WT/SOD1 but not Bax KO/SOD1 mutants (arrowheads, top), is markedly upregulated at P60 in both genotypes, and is maintained until end stage in Bax KO/SOD1 but not Bax WT/SOD1 mutants (arrowheads, bottom). Ovals surround the ventral horn. Scale bar, 100 μm. ***B***, Higher-power image of cytoplasmic mutant SOD1 expression around an MN nucleus (arrowhead). Scale bar, 25 μm. ***C***, Quantification of MNs with intense cytoplasmic mutant SOD1 expression (mutant SOD1-positive aggregates). $^{*}p < 0.01$, respective SOD1 versus P25 SOD1 mutant; $^{\dagger}p < 0.05$, Bax KO/SOD1 versus age-matched Bax WT/SOD1 mutant (the number of MNS with aggregates/section was averaged from 10 sections/animal; $n = 3–4$, each group). ***D***, Eighty-three percent atrophic (arrow) versus 0% healthy (arrowhead) YFP-expressing MNs express mutant SOD1 (20 YFP cells of each morphology examined per animal; $p < 0.001$; $n = 3$ at P40). Scale bar, 100 μm. ***E***, Mutant SOD1 immunoreactivity is expressed by motor axons in a region of the ventrolateral spinal cord, the width of which is measured by white bars in each image. White dots delimit the ventrolateral border of the ventral horn ($n = 3$, each group). Scale bar, 200 μm. Error bars indicate SDs.

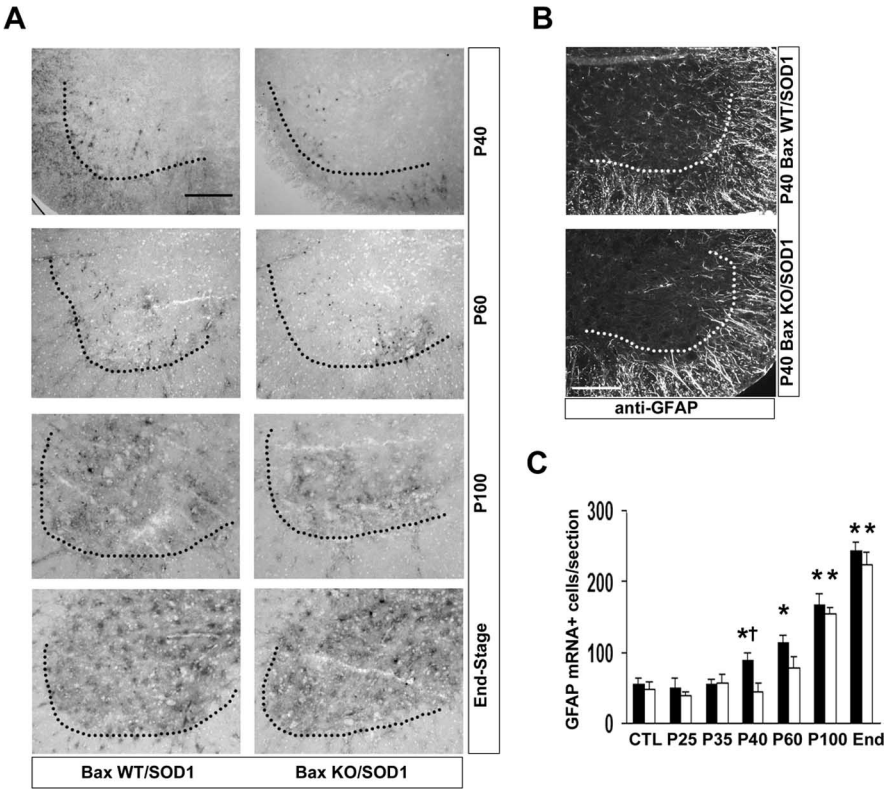

Figure 6. The increase of GFAP mRNA-positive cells in the spinal cord of SOD1 mutants is initiated after neuromuscular denervation and is delayed in the absence of Bax. ***A–C***, Significant increase in expression of GFAP mRNA (***A***, ***C***) and protein (***B***) in the lumbar ventral horn at P40 in Bax WT/SOD1, but not until P100 in Bax KO/SOD1 mutants. Filled and open bars in ***C*** refer to the number of GFAP mRNA-positive cells in Bax WT/SOD1 and Bax KO/SOD1 mutants, respectively. $*p < 0.05$ (***C***), respective mutant versus P25 SOD1 mutant; $^{\dagger}p < 0.05$, Bax KO/SOD1 versus age-matched Bax WT/SOD1 mutant; two-way ANOVA ($n = 4$, each group). Scale bars: ***A***, ***B***, 100 μm. Error bars indicate SDs.

tein. Indeed, the observation that mutant SOD1 begins to accumulate (P30) after the onset of neuromuscular denervation (P25) suggests that SOD1 aggregation occurs after denervation. To investigate this idea further, we crossed Bax WT/SOD1 mice with mice containing a spectral variant of green fluorescent protein (YFP) expressed throughout the cell body and processes of a small subpopulation of MNs (Feng et al., 2000). We counted the number of lumbar YFP-positive MNs and labeled them as atrophic or healthy depending on their morphology; atrophic neurons were smaller in size and rounded. We noticed, in contrast to healthy YFP-positive MNs, which failed to express mutant SOD1 in aggregates, that atrophic YFP-positive MNs often coexpressed mutant SOD1 in this pattern at P40 (Fig. 5*D*). Finally, we noticed intense mutant SOD1 immunoreactivity in the ventrolateral white matter that includes motor axons traveling radially out from the ventral horn as well as rostrocaudally through this region before exiting into the ventral roots; this immunoreactivity colocalized with NF-L immunostaining and increased over a similar period of time as the accumulation of mutant SOD1 in the cell body (data not shown) (Fig. 5*E*). Together, these data suggest that MNs first lose contact from their target and then accumulate mutant SOD1 protein in their proximal nerve and soma, and that MNs in Bax KO/SOD1 mutants exhibit mutant SOD1 aggregates later because they denervate later than Bax WT/SOD1 mutants.

Bax deletion delays reactive gliosis, which occurs after denervation

Experimental denervation of adult MNs from the target muscle results in an increase in the number of astrocytes proximal to affected MN cell bodies (Graeber and Kreutzberg, 1986). Because spinal cord and brain astrogliosis is a prominent feature in ALS, and because glial expression of molecules regulating excitotoxicity is downregulated in ALS (Rothstein et al., 1995), we next determined whether such astrogliosis occurred before or after the earliest denervation (P25) was detected in Bax WT/SOD1 mutants. Because the quantification of astrocyte-specific immunoreactive markers, such as GFAP, is difficult because of the elaborate extension of glial processes, we made a riboprobe and counted GFAP mRNA-positive, Hoechst-labeled nuclei in the ventral horn of Bax WT/SOD1 and Bax KO/SOD1 mutants at various ages. We observed a significant increase in the number of GFAP mRNA-positive cells in Bax WT/SOD1 mutants at P40, significantly earlier than previous reports of increases in GFAP immunoreactivity (Hall et al., 1998); Bax KO/SOD1 mutants failed to display an increase in astrocyte number until P60 (Fig. 6*A–C*). Nevertheless, by end stage this number was similar between genotypes, despite the absence of MN death in Bax KO/SOD1 mice. We observed two types of astrocytes in SOD1 mutant spinal cord: an initial increase in the number of small GFAP mRNA-positive nuclei (P40–P60 in Bax WT/SOD1 mutants) followed by a secondary increase in larger mRNA-labeled nuclei, often occurring in focal regions of the ventral horn (Fig. 6*A*, compare P60 to end-stage Bax KO/SOD1 mutant). Whether these two types of astroglia represent two different populations (i.e., resident vs foreign) or the same population at different stages of activation is unclear. Therefore, similar to (but later than) increased levels of mutant SOD1 accumulation in MN cell bodies, increases in the number of spinal astrocytes occur after the onset of denervation in Bax WT/SOD1 mutants, and are delayed in Bax KO/SOD1 mutants.

Bax deletion fails to inhibit mitochondrial vacuolization within NMJs

We next determined the time course of mitochondrial morphology in the spinal cord, ventral roots, and presynaptic terminals of SOD1 mutant mice. Because mitochondrial vacuolization peaks between P60–P100 in SOD1 G93A mutants (Kong and Xu, 1998), we first examined semithin sections of the lumbar ventral spinal cord at P100 and observed massive vacuolization in both Bax WT/SOD1 and Bax KO/SOD1 mutants (Fig. 7*A*). To determine whether vacuolization is differentially affected by neuromuscular denervation and hence Bax deletion, we examined the ventral spinal cord for vacuolated mitochondria at P25 (Bendotti et al., 2001). Although both mutant genotypes appeared indistinguishable from age-matched nonmutant controls in semithin sections, ultrastructural analysis confirmed the presence of vacuolated mitochondria in both SOD1 mutant genotypes (data not shown). We next examined electron photomicrographs of NMJs in the MG at P25 and quantified both the size and degree of vacuolization within presynaptic mitochondria (Hirai et al.,

2001). Whereas the overall area was unaffected, the percent area of each mitochondrion containing clear space, a marker of presumptive vacuolization, was significantly greater in Bax WT/SOD1 mutant than in Bax WT presynaptic terminals (32 ± 16 vs 8 ± 4; $n = 3$; $p < 0.01$). In contrast, preliminary analysis of Bax KO/SOD1 mutants ($n = 1$) demonstrated that neither the size nor area of vacuolization (11 ± 8) of presynaptic mitochondria was affected. We failed to observe mitochondrial alterations in muscle in any genotype (Fig. 7*B*). These results demonstrate that mitochondrial pathology within MN presynaptic terminals exists at the onset of neuromuscular denervation in Bax WT/SOD1 mutants.

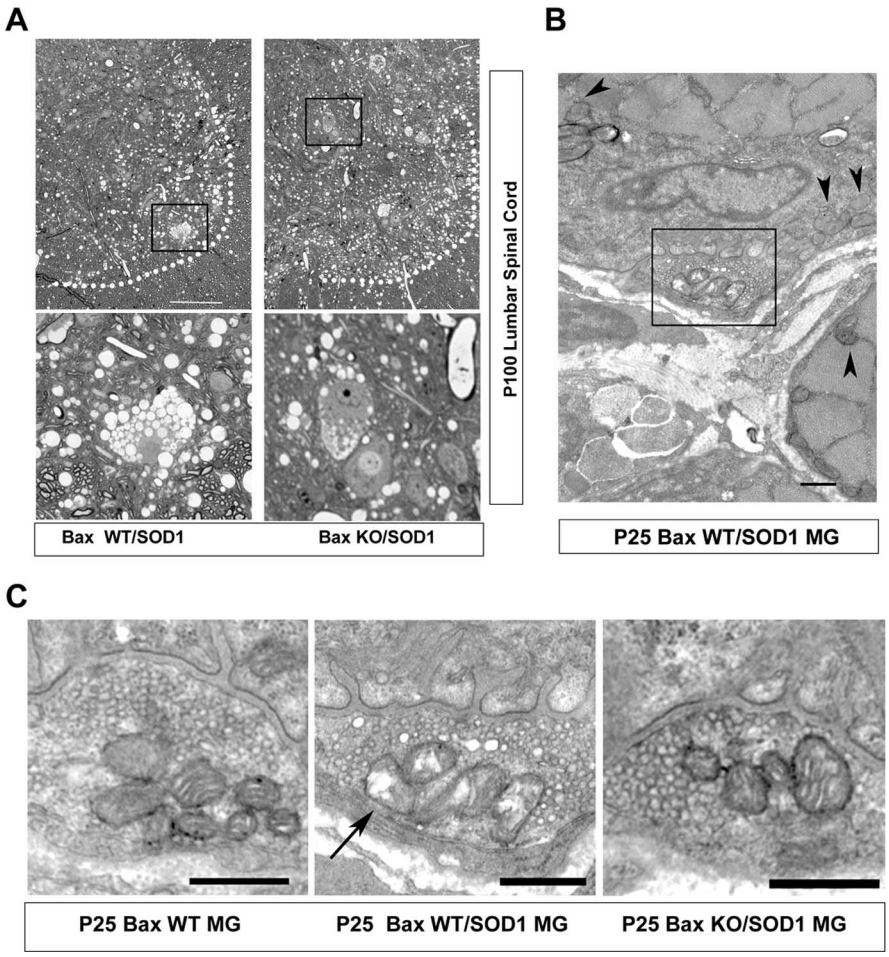

Figure 7. Bax deletion delays mutant SOD1-mediated mitochondrial vacuolization within MN presynaptic terminals. ***A***, Representative 1-μm-thick sections of the lumbar ventral horn exhibit massive vacuolization within the spinal cord at P100 in both Bax WT/SOD1 and Bax KO/SOD1 mutants ($n = 3$). The bottom panel is an enlarged image of the inset box in the top panel. Scale bar, 100 μm. ***B***, Electron micrograph of NMJ (box) within the MG in a Bax WT/SOD1 mutant at P25 shows normal-appearing mitochondria within muscle cells (arrowheads). Scale bar, 0.5 μm. ***C***, Clear vacuoles (arrow) in mitochondria of presynaptic terminals of MG-innervating MNs in Bax WT/SOD1 mutants but not Bax KO/SOD1 mutants or Bax WT at P25. Mean mitochondrial area: 187 ± 84 nm^2, Bax WT, $n = 5$; 186 ± 91 nm^2, Bax WT/SOD1, $n = 5$; $184 + 80$ nm^2, Bax KO/SOD1, $n = 1$; $p > 0.9$, Bax WT versus Bax WT/SOD1 (at least 15 mitochondria within 5 NMJs analyzed; ***C***) Scale bars, 0.5 μm. Box in ***B*** is enlarged in the middle panel of ***C***.

Mutant SOD1 protein is detected in MN presynaptic terminals and Schwann cells

Although Bax KO/SOD1 mutants exhibited increased evidence of sprouting, distal MN presynaptic axons failed to fully innervate muscle endplates. In many cases, axons grew near nAchR clusters but failed to stop and elaborate presynaptic elements (Fig. 8*A*). Nearly all such axons at end stage expressed GAP-43, suggesting that they are collateral sprouts (data not shown). These data prompted us to analyze expression of mutant SOD1 in distal axons. We observed mutant SOD1-positive MN presynaptic terminals in the MG at every age examined in both mutant genotypes (Fig. 8*B*), but could not detect WT SOD1 immunoreactivity in either mutants or wild-type controls (data not shown). Mutant SOD1 expression at NMJs is nonoverlapping with α-bungarotoxin-labeled nAChR clusters and appears punctuate, consistent with a presynaptic mitochondrial localization (Fig. 8*C*). We also detected mutant SOD1 in crude mitochondrial fractions derived from the spinal cord and peripheral nerve at P30, but failed to observe a difference in levels between Bax WT/SOD1 and Bax KO/SOD1 mutants (data not shown). Alternatively, mutant SOD1 expression in the NMJ might interact with synaptic proteins. Supporting this idea, we detected synaptophysin in mutant SOD1 immunoprecipitates. However, we also observed this protein in IgG precipitates (Fig. 9), raising a question as to whether mutant SOD1 specifically interacts with synaptic vesicles and/or with synaptic mitochondria. Together with the recent report that mutant SOD1 is imported into MN mitochondria (Liu et al., 2004), these data suggest that mutant SOD1 within the MN presynaptic terminal may contribute directly to denervation and/or the failure of successful reinnervation.

One of the most intriguing findings in transgenic models of FALS is the requirement for expression of mutant SOD1 by cell types other than MNs (Clement et al., 2003). If MN expression of mutant SOD1 in presynaptic terminals is required for but is insufficient to initiate axonal denervation and disease, what other cell type might be necessary to facilitate this pathogenetic process? When we stained sections of P45 Bax WT/SOD1 MG muscle with an antibody to S100, which labels both nerve- and NMJ-associated Schwann cells, we noticed that many but not all perisynaptic cells that exhibit mutant SOD1 immunoreactivity also express S100 (Fig. 8*D*). Many SOD1 immunoreactive terminal Schwann cells at P45 extended processes across multiple muscle fibers, an observation consistent with their role in "bridging" denervated and innervated synapses after experimental denervation (Fig. 8*D*) (Son and Thompson, 1995). We observed S100-immunoreactive terminal Schwann cells as early as P3, before the onset of MN denervation, and we detected no SOD1 immunoreactivity in terminal Schwann cells in Bax WT or Bax KO animals (data not shown) (Fig. 8*E*). Although such expression in Schwann cells need not be toxic, the proximity of these cells to the NMJ makes them attractive candidates for mediating cell nonautonomous effects of mutant SOD1 on MN presynaptic terminals.

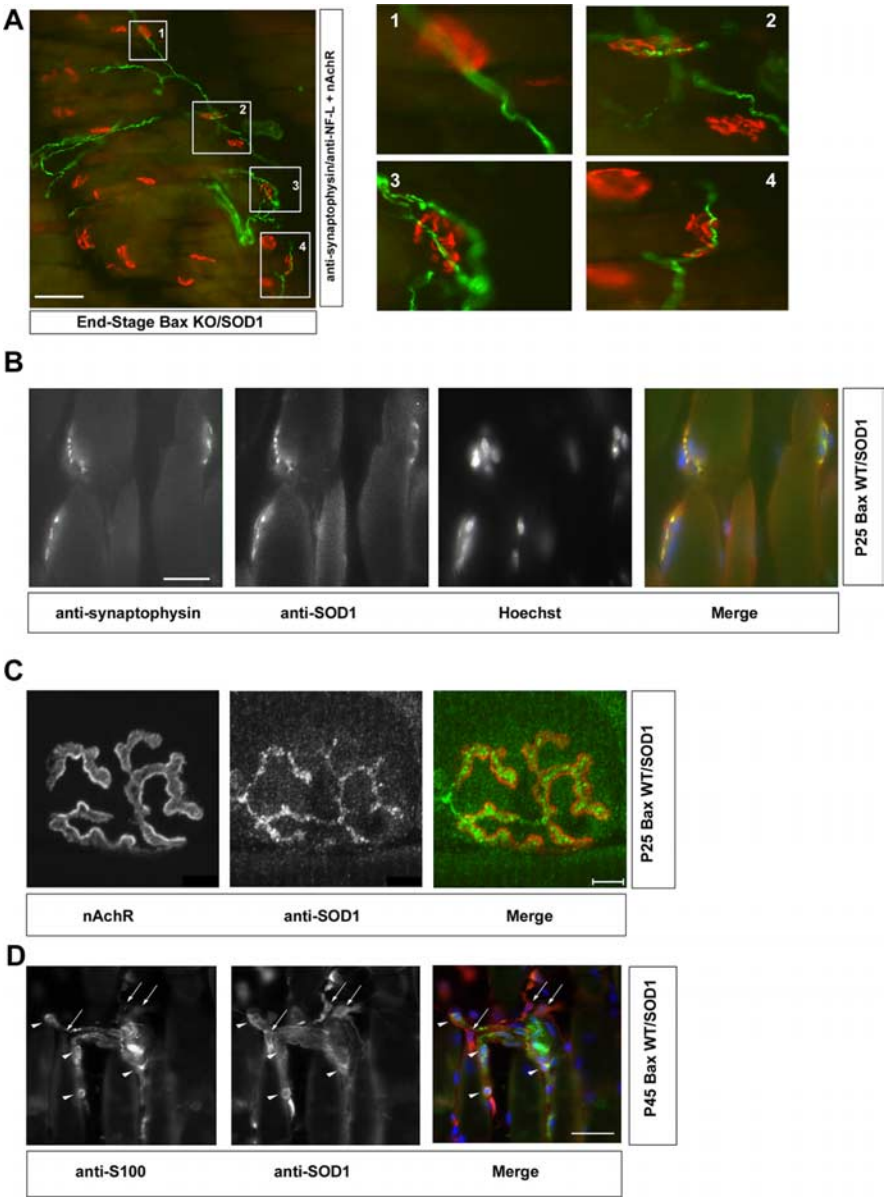

Figure 8. Mutant SOD1 is expressed in MN presynaptic terminals and terminal Schwann cells. ***A***, Lower (left) and higher (right) photomicrographs of NF-L- and synaptophysin (SYN)-labeled motor axons (green) and α-bungarotoxin (BTX)-labeled nAChRs (red) in the MG of end-stage Bax KO/SOD1 mutants. Higher-power images show four examples of axons traversing near but not terminating onto nAChR clusters. Scale bar, 150 μm. ***B***, Colocalization of SYN and mutant SOD1 in P25 Bax WT/SOD1 MG. Scale bar, 50 μm. ***C***, Mutant SOD1 does not colocalize with BTX at the NMJ in P25 Bax WT/SOD1 MG. Scale bar, 5 μm. ***D***, Colocalization of mutant SOD1 and S100 in P45 Bax WT/SOD1 MG. Arrowheads point to double-labeled cells, arrows to mutant SOD1-positive, S100-negative cells. Scale bar, 50 μm.

Discussion

Complete dissociation between MN death and denervation

Here, we provide the first definitive evidence that MN death is not required for disease in an animal model of ALS. Our results instead support the idea that peripheral denervation is the predominant pathological feature of MN disease (Fischer et al., 2004). This is significant because many of the prevailing hypotheses, including SOD1 accumulation and mitochondrial dysfunction, have been considered from the perspective of cell death activation (Bruijn et al., 1998; Liu et al., 2004). Although this study is the first to completely dissociate MN death from MN dysfunction in a model of MN disease, previous studies have demonstrated deficits in the distal MN that significantly precede or occur independently of cell death (Sagot et al., 1995; Fischer et al., 2004; Pagani et al., 2006; Pun et al., 2006). Such a dissociation between synaptic and cell body loss observed in Bax KO/SOD1 mutant MNs is also consistent with the results of trophic deprivation or injury studies (Deckwerth and Johnson, 1994; Mattson et al., 1998; Raff et al., 2002; Berliocchi et al., 2005). Finally, our results suggest that although denervating motor neuropathies may differ from MN disease by activating cell death pathways, therapeutic strategies aimed at disrupting common mechanisms of denervation may be more effective than those aimed at blocking cell death. Indeed, a recent study showing impaired mitochondrial function and retrograde transport in an animal model of hereditary spastic paraplegia suggests a striking similarity in the etiology of synaptic denervation between these two types of MN disorders (Ferreirinha et al., 2004). Nevertheless, mice with different forms of MN disease respond markedly differently to at least one strategy to reduce axonal degeneration, suggesting that the mechanisms that underlie synaptic denervation may vary between such diseases (Ferri et al., 2003; Vande Velde et al., 2004).

Bax deletion is unlikely to have extended the lifespan of ALS mutants by attenuating MN death, because disease still occurs in the absence of cell death and because the increase in lifespan is equivalent to the delay in motor decline. Nevertheless, we cannot exclude the possibility that such an increase in longevity represents a delay in the downstream effects of cell death activation, including neuromuscular denervation itself. However, this seems unlikely, because the upregulation of Bax protein levels and the onset of cell death occur >30 d later than the onset of NMJ denervation. Together with the observation that degeneration of MNs in SOD1 mutants progresses distally to proximally (Fischer et al., 2004), we favor the idea that Bax deletion extends SOD1 mutant survival not through delaying cell death but rather through retarding denervation. However, our results do not allow us to exclude the possibility that a centrally initiated insult (e.g., astroglia or microglia) results in the disruption of distal MN transport and subsequent denervation (Raff et al., 2002).

One such mechanism by which Bax may delay MN denervation is through an early increase in the number of muscle-innervating MNs because of the inhibition of developmental cell death. This explanation seems unlikely, however, because whereas Bax deletion and Bcl-2 overexpression both extend lifespan of SOD1 mutant mice by 15%, transgenic overexpression of Bcl-2 is initiated postnatally and, thus, does not prevent develop-

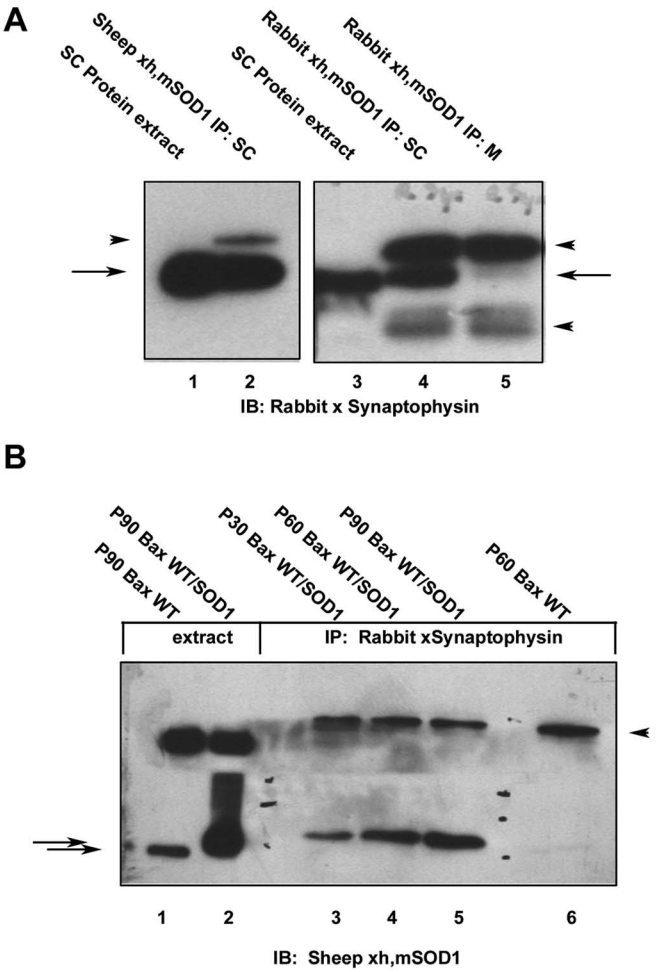

Figure 9. ***A***, Synaptophysin (SYN) is present in mutant SOD1 IPs of P100 Bax WT/SOD1 mutant protein extract, using either sheep (left) or rabbit antibodies (right). SC, Spinal cord; M, muscle. Arrowheads point to IgG and arrows to SYN (38 kDa). ***B***, Mutant but not WT SOD1 is present in SYN IPs of Bax WT/SOD1 mutant (lanes 3–5) or Bax WT (lane 6) muscle extract. Arrowhead points to IgG heavy chain and arrows to human and mouse SOD1.

mental MN death (Kostic et al., 1997). Additionally, because the number of both total and innervated postsynaptic nAchR receptors is similar in Bax WT and Bax KO muscles, it is unlikely that Bax deletion extended survival of SOD1 mutants through the initial presence of extra synapses.

Denervation is delayed in Bax KO/SOD1 mutants and precedes mutant SOD1 accumulation and gliosis

The early withdrawal of innervated synapses in the MG of Bax WT/SOD1 mutants (P25) prompted us to examine several other disease processes in both genotypes that may contribute to denervation. We first detected mutant SOD1-immunoreactive aggregates shortly after the onset of denervation, suggesting that SOD1 exerts its toxicity at the synapse before forming aggregates in the cell body. Interestingly, a recent report demonstrated that a physical interaction between mutant SOD1 and chromogranins mediates secretion of mutant SOD1 (Urushitani et al., 2006). Because chromogranins have also been detected in motor nerve terminals (Booj et al., 1989), we speculate that the early loss of innervation interferes with the ability of MNs to export mutant SOD1, resulting in the proximal accumulation and subsequent aggregation of this protein. Alternatively, the formation of aggregates may represent an attempt by denervating MNs to sequester mutant SOD1 and thereby ameliorate its toxicity (Taylor et al., 2003).

The increase in SOD1 immunoreactivity after denervation was paralleled by a similar increase in astrogliosis in the spinal cord, consistent with the notion that glial cells are upregulated in MN diseases in response to neuromuscular denervation. Together, our findings that SOD1 accumulation and astrogliosis occur after denervation and are delayed in Bax KO/SOD1 mutants suggest that these two processes are not likely to drive MN dysfunction. However, these results cannot rule out the possibility that SOD1 accumulation in other compartments, such as the axon or synapse, mediates MN degeneration, nor can they disprove a toxic role for glia independent of astrogliosis.

Synaptic and perisynaptic expression of SOD1 and altered mitochondria in presynaptic MN terminals

The early loss of innervated neuromuscular synapses identifies MN presynaptic terminals as one potential locus of mutant SOD1-mediated toxicity. Consistent with this idea, we observed intense mutant SOD1 immunoreactivity in MN terminals at every age examined. Although the precise subsynaptic expression of mutant SOD1 remains unknown, the relative abundance of presynaptically localized mitochondria, together with the demonstration that mutant SOD1 is associated selectively within the mitochondria of MNs (Liu et al., 2004), indicates this organelle as a likely source. Alternatively, mutant SOD1 may be directly associated with either synaptic vesicles or synaptically located large dense-core vesicles (Urushitani et al., 2006), a possibility that is supported by the interaction between synaptophysin and mutant SOD1. Additional evidence that mutant SOD1 may impair synaptic function is provided by the recent demonstration that synaptic vesicle transport is impaired in SOD1 mutant motor axons even before distal synaptic loss (Pun et al., 2006). We thus envision three possibilities by which mutant SOD1 causes neuromuscular denervation: (1) mutant SOD1 expression within mitochondria disrupts the function of this organelle within MNs, leading first to the dysfunction of synapses, which depend on relatively large sources of metabolic energy (Guo et al., 2005; Verstreken et al., 2005); (2) expression in mitochondria provides synaptic access to mutant SOD1 and, thus, an opportunity to indirectly impair synaptic function; (3) mutant SOD1 association with synaptophysin impairs the transport or function of synaptic vesicles. Evidence consistent with the latter two possibilities includes the observation that dynein mutants that produce MN disease also redistribute mitochondria toward the nuclear periphery (Hafezparast et al., 2003; Varadi et al., 2004). Similarly, dynactin mutants that produce MN disease disrupt synaptic stabilization at the *Drosophila* NMJ (Eaton et al., 2002; LaMonte et al., 2002). Therefore, mutations in dynein/dynactin or SOD1 may impair the distribution, motility, or function of presynaptic mitochondria, thereby causing synaptic denervation.

Our argument that the loss of innervated synapses drives motor dysfunction in FALS mutant mice primarily results from the comparison between Bax WT/SOD1 and Bax KO/SOD1 mutants. The delay in both the onset of denervation and motor dysfunction is similar in length to the increase in lifespan, arguing strongly against a role for Bax in prolonging survival through affecting cell death. How then does Bax deletion delay the loss of innervated NMJs in SOD1 mutant mice? Because both Bax and the proapoptotic Bcl-2 family member Bak alter synaptic transmission (Fannjiang et al., 2003; Jonas et al., 2005), Bax expression may enhance the synaptic-destabilizing effects of mutant SOD1, perhaps by increasing the dysfunction of mitochondria or by

perturbing the transport or activity of synaptic vesicles. However, the subcellular fractionation studies argue against the possibility that Bax deficiency ameliorates mitochondrial dysfunction by reducing the levels of mitochondrial-associated mutant SOD1. Alternatively, Bax may regulate the process of reinnervation after injury (Chen et al., 1997). Interestingly, the ventral roots of Bax KO/SOD1 mutants contained more collateral axon sprouts and higher levels of GAP-43 expression than those of Bax WT/SOD1 mutants, supporting this idea. Because the capacity for compensatory reinnervation appears restricted to subsets of MNs in the SOD1 mutant (Frey et al., 2000; Schaefer et al., 2005; Pun et al., 2006), Bax deletion may increase the size of this population and therefore increase reinnervation in SOD1 mutants.

A recent report demonstrated that MNs themselves are not likely the source of the mutant SOD1 that causes MN degeneration (Clement et al., 2003). Our localization of mutant SOD1 in perisynaptic Schwann cells suggests the possibility that mutant SOD1 expression in these cells causes either an insult to or impairs the trophic maintenance of normal or regenerating motor axons (Son and Thompson, 1995). One candidate for such a Schwann cell-derived trophic molecule is VEGF, which Schwann cells upregulate after injury (Gupta et al., 2005), and mutations of which cause ALS (Lambrechts et al., 2003). It therefore seems plausible that disruptions of MN axonal transport or synaptic function caused by MN-derived mutant SOD1 require a compounding deficit in Schwann cell-mediated reinnervation in order for MNs to succumb to ALS. In summary, our data suggest that toxicity to MNs caused by mutant SOD1 is mediated through the disruption of MN presynaptic terminals rather than through the activation of cell death, and as such may aid in the development of therapies designed to preserve motor function in MN diseases.

References

Bendotti C, Calvaresi N, Chiveri L, Prelle A, Moggio M, Braga M, Silani V, De Biasi S (2001) Early vacuolization and mitochondrial damage in motor neurons of FALS mice are not associated with apoptosis or with changes in cytochrome oxidase histochemical reactivity. J Neurol Sci 191:25–33.

Berliocchi L, Fava E, Leist M, Horvat V, Dinsdale D, Read D, Nicotera P (2005) Botulinum neurotoxin C initiates two different programs for neurite degeneration and neuronal apoptosis. J Cell Biol 168:607–618.

Booj S, Goldstein M, Fischer-Colbrie R, Dahlstrom A (1989) Calcitonin gene-related peptide and chromogranin A: presence and intra-axonal transport in lumbar motor neurons in the rat, a comparison with synaptic vesicle antigens in immunohistochemical studies. Neuroscience 30: 479–501.

Bruijn LI, Houseweart MK, Kato S, Anderson KL, Anderson SD, Ohama E, Reaume AG, Scott RW, Cleveland DW (1998) Aggregation and motor neuron toxicity of an ALS-linked SOD1 mutant independent from wild-type SOD1. Science 281:1851–1854.

Chen DF, Schneider GE, Martinou JC, Tonegawa S (1997) Bcl-2 promotes regeneration of severed axons in mammalian CNS. Nature 385:434–439.

Chiesa R, Piccardo P, Dossena S, Nowoslawski L, Roth KA, Ghetti B, Harris DA (2005) Bax deletion prevents neuronal loss but not neurological symptoms in a transgenic model of inherited prion disease. Proc Natl Acad Sci USA 102:238–243.

Chiu AY, Zhai P, Dal Canto MC, Peters TM, Kwon YW, Prattis SM, Gurney ME (1995) Age-dependent penetrance of disease in a transgenic mouse model of familial amyotrophic lateral sclerosis. Mol Cell Neurosci 6:349–362.

Clement AM, Nguyen MD, Roberts EA, Garcia ML, Boillee S, Rule M, McMahon AP, Doucette W, Siwek D, Ferrante RJ, Brown Jr RH, Julien JP, Goldstein LS, Cleveland DW (2003) Wild-type nonneuronal cells extend survival of SOD1 mutant motor neurons in ALS mice. Science 302:113–117.

Cleveland DW, Rothstein JD (2001) From Charcot to Lou Gehrig: deciphering selective motor neuron death in ALS. Nat Rev Neurosci 2:806–819.

Deckwerth TL, Johnson Jr EM (1994) Neurites can remain viable after destruction of the neuronal soma by programmed cell death. Dev Biol 165:63–72.

Eaton BA, Fetter RD, Davis GW (2002) Dynactin is necessary for synapse stabilization. Neuron 34:729–741.

Fannjiang Y, Kim CH, Huganir RL, Zou S, Lindsten T, Thompson CB, Mito T, Traystman RJ, Larsen T, Griffin DE, Mandir AS, Dawson TM, Dike S, Sappington AL, Kerr DA, Jonas EA, Kaczmarek LK, Hardwick JM (2003) BAK alters neuronal excitability and can switch from anti- to prodeath function during postnatal development. Dev Cell 4:575–585.

Feng G, Mellor RH, Bernstein M, Keller-Peck C, Nguyen QT, Wallace M, Nerbonne JM, Lichtman JW, Sanes JR (2000) Imaging neuronal subsets in transgenic mice expressing multiple spectral variants of GFP. Neuron 28:41–51.

Ferreirinha F, Quattrini A, Pirozzi M, Valsecchi V, Dina G, Broccoli V, Auricchio A, Piemonte F, Tozzi, G, Gaeta L, Casari G, Ballabio A, Rugarli EI (2004) Axonal degeneration in paraplegin-deficient mice is associated with abnormal mitochondria and impairment of axonal transport. J Clin Inv 113:231–242.

Ferri A, Sanes JR, Coleman MP, Cunningham JM, Kato AC (2003) Inhibiting axon degeneration and synapse loss attenuates apoptosis and disease progression in a mouse model of motoneuron disease. Curr Biol 13:669–673.

Fischer LR, Culver DG, Tennant P, Davis AA, Wang M, Castellano-Sanchez A, Khan J, Polak MA, Glass JD (2004) Amyotrophic lateral sclerosis is a distal axonopathy: evidence in mice and man. Exp Neurol 185:232–240.

Frey D, Schneider C, Xu L, Borg J, Spooren W, Caroni P (2000) Early and selective loss of neuromuscular synapse subtypes with low sprouting competence in motoneuron diseases. J Neurosci 20:2534–2542.

Gould TW, Oppenheim RW (2004) The function of neurotrophic factor receptors expressed by the developing adductor motor pool *in vivo*. J Neurosci 24:4668–4682.

Graeber MB, Kreutzberg GW (1986) Astrocytes increase in glial fibrillary acidic protein during retrograde changes of facial motor neurons. J Neurocytol 15:363–373.

Green DR, Reed JC (1998) Mitochondria and apoptosis. Science 281: 1309–1312.

Guégan C, Przedborski S (2003) Programmed cell death in amyotrophic lateral sclerosis. J Clin Invest 111:153–161.

Guo X, Macleod GT, Wellington A, Hu F, Panchumarthi S, Schoenfield M, Marin L, Charlton MP, Atwood HL, Zinsmaier KE (2005) The GTPase dMiro is required for axonal transport of mitochondria to *Drosophila* synapses. Neuron 47:379–393.

Gupta R, Gray M, Chao T, Bear D, Modafferi E, Mozaffar T (2005) Schwann cells upregulate vascular endothelial growth factor secondary to chronic nerve compression injury. Muscle Nerve 31:452–460.

Gurney ME, Haifeng P, Chiu AY, Dal Canto MC, Polchow Y, Alexander DD, Caliendo J, Hentati A, Kwon YW, Deng H, Chen W, Zhai P, Sufit RL, Siddique T (1994) Motor neuron degeneration in mice that express a human Cu, Zn superoxide dismutase mutation. Science 264:1772–1775.

Hafezparast M, Klocke R, Ruhrberg C, Marquardt A, Ahmad-Annuar A, Bowen S, Lalli G, Witherden AS, Hummerich H, Nicholson S, Morgan PJ, Oozageer R, Priestley JV, Averill S, King VR, Ball S, Peters J, Toda T, Yamamoto A, Hiraoka Y, et al. (2003) Mutations in dynein link motor neuron degeneration to defects in retrograde transport. Science 300:808–812.

Hall ED, Oostveen JA, Gurney ME (1998) Relationship of microglial and astrocytic activation to disease onset and progression in a transgenic model of familial ALS. Glia 23:249–256.

Hanyu N, Oguchi K, Yanagisawa N, Tsukagoshi H (1982) Degeneration and regeneration of ventral root motor fibers in amyotrophic lateral sclerosis. Morphometric studies of cervical ventral roots. J Neurol Sci 55:99–115.

Heads T, Pollock M, Robertson A, Sutherland WH, Allpress S (1991) Sensory nerve pathology in amyotrophic lateral sclerosis. Acta Neuropathol (Berl) 82:316–320.

Hirai K, Aliev G, Nunomura A, Fujioka H, Russell RL, Atwood CS, Johnson AB, Kress Y, Vinters HV, Tabaton M, Shimohama S, Cash AD, Siedlak SL, Harris PL, Jones PK, Petersen RB, Perry G, Smith MA (2001) Mitochondrial abnormalities in Alzheimer's disease. J Neurosci 21:3017–3023.

Johnston JA, Ward CL, Kopito RR (1998) Aggresomes: a cellular response to misfolded proteins. J Cell Biol 143:1883–1898.

Johnston JA, Dalton MJ, Gurney ME, Kopito RR (2000) Formation of high

molecular weight complexes of mutant Cu, Zn-superoxide dismutase in a mouse model for familial amyotrophic lateral sclerosis. Proc Natl Acad Sci USA 97:12571–12576.

Jonas EA, Hardwick JM, Kaczmarek LK (2005) Actions of BAX on mitochondrial channel activity and on synaptic transmission. Antioxid Redox Signal 7:1092–1100.

Kang SJ, Sanchez I, Jing N, Yuan J (2003) Dissociation between neurodegeneration and caspase-11-mediated activation of caspase-1 and caspase-3 in a mouse model of amyotrophic lateral sclerosis. J Neurosci 23:5455–5460.

Kennel PF, Finiels F, Revah F, Mallet J (1996) Neuromuscular function impairment is not caused by motor neurone loss in FALS mice: an electromyographic study. NeuroReport 7:1427–1431.

Kirkinezos IG, Bacman SR, Hernandez D, Oca-Cossio J, Arias LJ, Perez-Pinzon MA, Bradley WG, Moraes CT (2005) Cytochrome c association with the inner mitochondrial membrane is impaired in the CNS of G93A-SOD1 mice. J Neurosci 25:164–172.

Knudson CM, Tung KS, Tourtellotte WG, Brown GA, Korsmeyer SJ (1995) Bax-deficient mice with lymphoid hyperplasia and male germ cell death. Science 270:96–99.

Kong J, Xu Z (1998) Massive mitochondrial degeneration in motor neurons triggers the onset of amyotrophic lateral sclerosis in mice expressing a mutant SOD1. J Neurosci 18:3241–3250.

Kostic V, Jackson-Lewis V, de Bilbao F, Dubois-Dauphin M, Przedborski S (1997) Bcl-2: prolonging life in a transgenic mouse model of familial amyotrophic lateral sclerosis. Science 277:559–562.

Lambrechts D, Storkebaum E, Morimoto M, Del-Favero J, Desmet F, Marklund SL, Wyns S, Thijs V, Andersson J, van Marion I, Al-Chalabi A, Bornes S, Musson R, Hansen V, Beckman L, Adolfsson R, Pall HS, Prats H, Vermeire S, Rutgeerts P, et al. (2003) VEGF is a modifier of amyotrophic lateral sclerosis in mice and humans and protects motoneurons against ischemic death. Nat Genet 34:383–394.

LaMonte BH, Wallace KE, Holloway BA, Shelly SS, Ascano J, Tokito M, Van Winkle T, Howland DS, Holzbaur EL (2002) Disruption of dynein/dynactin inhibits axonal transport in motor neurons causing late-onset progressive degeneration. Neuron 34:715–727.

Ligon LA, LaMonte BH, Wallace KE, Weber N, Kalb RG, Holzbauer EL (2005) Mutant superoxide dismutase disrupts cytoplasmic dynein in motor neurons. NeuroReport 16:533–536.

Liu J, Lillo C, Jonsson PA, Vande Velde C, Ward CM, Miller TM, Subramaniam JR, Rothstein JD, Marklund S, Andersen PM, Brannstrom T, Gredal O, Wong PC, Williams DS, Cleveland DW (2004) Toxicity of familial ALS-linked SOD1 mutants from selective recruitment to spinal mitochondria. Neuron 43:5–17.

Lubischer JL, Thompson WJ (1999) Neonatal partial denervation results in nodal but not terminal sprouting and a decrease in efficacy of remaining neuromuscular junctions in rat soleus muscle. J Neurosci 19:8931–8944.

Mattson MP, Keller JN, Begley JG (1998) Evidence for synaptic apoptosis. Exp Neurol 153:35–48.

Migheli A, Atzori C, Piva R, Tortarolo M, Girelli M, Schiffer D, Bendotti C (1999) Lack of apoptosis in mice with ALS. Nat Med 5:966–967.

Pagani MR, Reisin RC, Uchitel OD (2006) Calcium signaling pathways mediating synaptic potentiation triggered by amyotrophic lateral sclerosis IgG in motor nerve terminals. J Neurosci 26:2661–2672.

Pasinelli P, Houseweart MK, Brown Jr RH, Cleveland DW (2000) Caspase-1 and -3 are sequentially activated in motor neuron death in Cu, Zn superoxide dismutase-mediated familial amyotrophic lateral sclerosis. Proc Natl Acad Sci USA 97:13901–13906.

Pasinelli P, Belford ME, Lennon N, Bacskai BJ, Hyman BT, Trotti D, Brown Jr RH (2004) Amyotrophic lateral sclerosis-associated SOD1 mutant proteins bind and aggregate with Bcl-2 in spinal cord mitochondria. Neuron 43:19–30.

Pun S, Santos AF, Saxena S, Xu L, Caroni P (2006) Selective vulnerability and pruning of phasic motoneuron axons in motoneuron disease alleviated by CNTF. Nat Neurosci 9:408–419.

Raff MC, Whitmore AV, Finn JT (2002) Axonal self-destruction and neurodegeneration. Science 296:868–871.

Rosen DR, Siddique T, Patterson D, Figlewicz DA, Sapp P, Hentati A, Donaldson D, Goto J, O'Regan JP, Deng H, Rahmani Z, Krizus A, McKenna-Yasek D, Cayabyab A, Gaston SM, Berger R, Tanzi RE, Halperin JJ, Herzfeldt B, Van Den Bergh R, et al. (1993) Mutations in Cu/Zn superoxide dismutase gene are associated with familial amyotrophic lateral sclerosis. Nature 362:59–62.

Rothstein JD, Van Kammen M, Levey AI, Martin LJ, Kuncl RW (1995) Selective loss of glial glutamate transporter GLT-1 in amyotrophic lateral sclerosis. Ann Neurol 38:73–84.

Sagot Y, Dubois-Dauphin M, Tan SA, de Bilbao F, Aebischer P, Martinou JC, Kato AC (1995) Bcl-2 overexpression prevents motoneuron cell body loss but not axonal degeneration in a mouse model of a neurodegenerative disease. J Neurosci 15:7727–7733.

Schaefer AM, Sanes JR, Lichtman JW (2005) A compensatory subpopulation of motor neurons in a mouse model of amyotrophic lateral sclerosis. J Comp Neurol 490:209–219.

Smith RG, Siklos L, Alexianu ME, Engelhardt JI, Mosier DR, Colom L, Habib Mohamed A, Appel SH (1996) Autoimmunity and ALS. Neurology 47:S40–S45.

Son YJ, Thompson WJ (1995) Schwann cell processes guide regeneration of peripheral axons. Neuron 14:125–132.

Sun W, Gould TW, Vinsant S, Prevette D, Oppenheim RW (2003) Neuromuscular development after the prevention of naturally occurring neuronal death by Bax deletion. J Neurosci 23:7298–7310.

Taylor JP, Tanaka F, Robitschek J, Sandoval CM, Taye A, Markovic-Plese S, Fischbeck KH (2003) Aggresomes protect cells by enhancing the degradation of toxic polyglutamine-containing protein. Hum Mol Genet 12:749–757.

Urushitani M, Sik A, Sakurai T, Nukina N, Takahashi R, Julien JP (2006) Chromogranin-mediated secretion of mutant superoxide dismutase proteins linked to amyotrophic lateral sclerosis. Nat Neurosci 9:108–118.

Vande Velde C, Garcia ML, Yin X, Trapp BD, Cleveland DW (2004) The neuroprotective factor Wlds does not attenuate mutant SOD1-mediated motor neuron disease. Neuromolecular Med 5:193–203.

Varadi A, Johnson-Cadwell LI, Cirulli V, Yoon Y, Allan VJ, Rutter GA (2004) Cytoplasmic dynein regulates the subcellular distribution of mitochondria by controlling the recruitment of the fission factor dynamin-related protein-1. J Cell Sci 117:4389–4400.

Verstreken P, Ly CV, Venken KJ, Koh TW, Zhou Y, Bellen HJ (2005) Synaptic mitochondria are critical for mobilization of reserve pool vesicles at Drosophila neuromuscular junctions. Neuron 47:365–378.

Vukosavic S, Dubois-Dauphin M, Romero N, Przedborski S (1999) Bax and Bcl-2 interaction in a transgenic mouse model of familial amyotrophic lateral sclerosis. J Neurochem 73,:2460–2468.

Wong PC, Pardo CA, Borchelt DR, Lee MK, Copeland NG, Jenkins NA, Sisodia SS, Cleveland DW, Price DL (1995) An adverse property of a familial ALS-linked SOD1 mutation causes motor neuron disease characterized by vacuolar degeneration of mitochondria. Neuron 14:1105–1116.